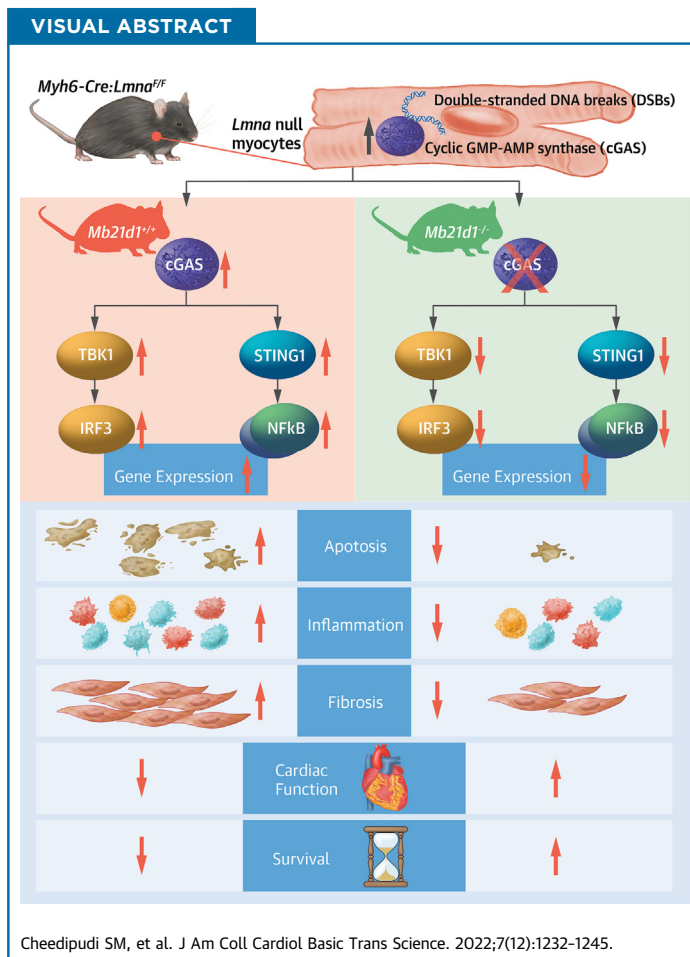


ORIGINAL RESEARCH - PRECLINICAL

Genetic Ablation of the DNA Damage Response Pathway Attenuates Lamin-Associated Dilated Cardiomyopathy in Mice



Sirisha M. Cheedipudi, PhD, Saman Asghar, BS, Ali J. Marian, MD



HIGHLIGHTS

- The LMNA protein is involved in genomic stability.
- Mutations in the *LMNA* gene caused DCM.
- DSBs are increased in DCM.
- DSBs, released into the cytoplasm, are sensed by CGAS, which activates STING1/TBK1 and results in activation of IRF3 and NFκB1 pathways.
- Activated IRF3 and NFκB1 induce expression of proinflammatory cytokines and contribute to the pathogenesis of DCM.
- Genetic ablation of cytosolic DNA sensor CGAS attenuates the LMNA-associated DCM phenotype in mice.

From the Center for Cardiovascular Genetics, Institute of Molecular Medicine, University of Texas Health Science Center, Houston, Texas, USA.

The authors attest they are in compliance with human studies committees and animal welfare regulations of the authors' institutions and Food and Drug Administration guidelines, including patient consent where appropriate. For more information, visit the [Author Center](#).

Manuscript received March 9, 2022; revised manuscript received June 17, 2022, accepted June 18, 2022.

SUMMARY

Hereditary dilated cardiomyopathy (DCM) is a primary disease of cardiac myocytes caused by mutations in genes encoding proteins with a diverse array of functions. Mutations in the *LMNA* gene, encoding the nuclear envelope protein lamin A/C, are the second most common causes of DCM. The phenotype is characterized by progressive cardiac dysfunction, leading to refractory heart failure, myocardial fibrosis, cardiac arrhythmias, and sudden cardiac death. The molecular pathogenesis of DCM caused by the *LMNA* mutations is not well known. The *LMNA* protein is involved in nuclear membrane stability. It is also a guardian of the genome involved in the processing of the topoisomerases at the transcriptionally active domain and the repair of double-stranded DNA breaks (DSBs). Deletion of the mouse *Lmna* gene in cardiac myocytes leads to premature death, DCM, myocardial fibrosis, and apoptosis. The phenotype is associated with increased expression of the cytosolic DNA sensor cyclic GMP-AMP synthase (CGAS) and activation of the DNA damage response (DDR) pathway. Genetic blockade of the DDR pathway, upon knockout of the *Mb21d1* gene encoding CGAS, prolonged survival, improved cardiac function, partially restored levels of molecular markers of heart failure, and attenuated myocardial apoptosis and fibrosis in the *LMNA*-deficient mice. The findings indicate that targeting the CGAS/DDR pathway might be beneficial in the treatment of DCM caused by mutations in the *LMNA* gene. (J Am Coll Cardiol Basic Trans Science 2022;7:1232-1245) © 2022 The Authors. Published by Elsevier on behalf of the American College of Cardiology Foundation. This is an open access article under the CC BY-NC-ND license (<http://creativecommons.org/licenses/by-nc-nd/4.0/>).

ABBREVIATIONS AND ACRONYMS

CGAS = cyclic GMP-AMP synthase
DCM = dilated cardiomyopathy
DDR = DNA damage response
DSB = double-stranded DNA break
IRF3 = interferon regulatory factor 3
LMNA = lamin A/C
NFκB1 = nuclear factor kappa B subunit 1
STING1 = stimulator of interferon 1
TBK1 = TANK-binding kinase 1

Hear failure is a leading cause of mortality and morbidity, affecting approximately 65 million people worldwide.^{1,2} Dilated cardiomyopathy (DCM) is a prototypic form of heart failure with reduced ejection fraction and a major indication for heart transplantation.³ Hereditary DCM is a genetically heterogeneous disease caused by mutations (pathogenic variants) in more than 2 dozen genes.⁴ Mutations of the *LMNA* gene encoding the lamin A/C protein (LMNA) are among the most common causes for hereditary DCM.^{5,6} There is no specific therapy for DCM caused by mutations in the *LMNA* gene.

The LMNA protein is expressed ubiquitously in almost all differentiated cells, including cardiac myocytes.⁷ LMNA, because of its topographic location within the nuclear inner membrane, interacts with chromatin and regulates gene expression.^{8,9} Given its ubiquitous expression and interactions with a large part of the chromatin, mutations in the *LMNA* gene cause more than a dozen distinct phenotypes, such as Hutchinson-Gilford progeria syndrome, muscular dystrophy, lipodystrophy, and restrictive dermopathy, among others, which are collectively referred to as laminopathies.^{10,11}

Several mechanisms are involved in the pathogenesis of the laminopathies, including dysregulated gene expression and altered mechanical properties of the nuclear membrane.^{10,12,13} Recently, induction of double-stranded DNA breaks (DSBs), release of the DSBs into the cytosol, and activation of the DNA damage response (DDR) pathway are implicated in the

pathogenesis of DCM in laminopathies.^{14,15} Activation of the DDR pathway, comprised of the cytosolic DNA sensor cyclic GMP-AMP synthase (CGAS) and its downstream effectors, stimulator of interferon 1 (STING1) and TANK-binding kinase 1 (TBK1), leads to expression of proinflammatory cytokines through the interferon regulatory factor 3 (IRF3) and the nuclear factor kappa B subunit 1 (NFκB1) pathways.¹⁶ Consequently, a proinflammatory milieu in the myocardium is established, which induces cell death and fibrosis, leading to cardiac dysfunction and heart failure. The purpose of the present study was to determine contributions of activation of the CGAS/DDR pathway to the pathogenesis of DCM caused by the LMNA deficiency in cardiac myocytes.

METHODS

ANESTHESIA AND EUTHANASIA. Echocardiography was performed under general anesthesia, which was induced with 3% inhaled isoflurane and maintained at 0.5%-1.0% isoflurane throughout the procedures. The mice were killed with CO₂ gas inhalation followed by cervical dislocation.

Myh6-Cre: *Lmna*^{F/F} MICE. Generation and phenotypic characterization of the *Myh6-Cre: Lmna*^{F/F} mice have been published.¹⁷ In brief, to delete the *Lmna* gene in cardiac myocytes, the mice with the floxed exon 2 of the *Lmna* gene (*Lmna*^{F/F}) were crossed to the *Myh6-Cre* transgenic mice, as published.¹⁷⁻¹⁹ Mice were housed in a 12-hour light/dark cycle facility with food and water available ad libitum.

Genomic DNA was extracted from tail clips and used for genotyping. In brief, the mouse tails were incubated with 50 μ L extraction buffer and 12.5 μ L tissue preparation solution (Sigma, cat. nos. E7526 and T3073) on a 55 °C water bath for 10 minutes followed by incubation at 95 °C for 3 minutes. Neutralization solution was added to the samples before polymerase chain reaction (PCR). An aliquot of 2 μ L of the solution containing tail DNA from each sample was used along with REExtract-N-AMP PCR Ready Mix (Sigma, cat. no. R4775) for genotyping. The list of the oligonucleotide primers used for genotyping is presented in [Supplemental Table 1](#).

B6(C)-Cgastm^{1d(EUCOMM)Hm9u/J} OR *Mb21d1* (CGAS) KNOCKOUT MICE (JAX STRAIN NO. 026554). These mice lack exon 2 of the *Mb21d1* gene, which is removed with the use of Cre-recombinase followed by the subsequent excision of the Cre recombinase transgene.²⁰

SURVIVAL. Survival of male and female wild-type (WT), *Myh6-Cre*, *Mb21d1*^{-/-}, *Myh6-Cre:Lnna*^{F/F}, and *Myh6-Cre:Lnna*^{F/F}:*Mb21d1*^{-/-} mice were analyzed by means of Kaplan-Meier survival curves.

ECHOCARDIOGRAPHY. Cardiac function was assessed by means of echocardiography with the use of a Vevo 1100 ultrasound imaging system (Fujifilm VisualSonics), as published.^{15,17,21-23} Male and female mice were anesthetized with the use of 1% isoflurane and heart rate maintained at 500 beats/min. M-mode images were obtained, and a leading-edge method was used to measure the interventricular septal thickness (IVST), posterior wall thickness (PWT), left ventricular end-diastolic diameter (LVEDD), and left ventricular end-systolic diameter (LVESD) in 5 to 6 cardiac cycles, and mean values were used. Using the measured parameters, the left ventricular fractional shortening (LVFS) and left ventricular mass were calculated. For calculating the left ventricular mass, the following formula was used²⁴: [(IVST + LVEDD + PWT) \times (IVST + LVEDD + PWT) \times (IVST + LVEDD + PWT) - (LVEDD \times LVEDD \times LVEDD) \times 1.04 \times 0.80]. Left ventricular mass was divided by body weight to obtain left ventricular mass index (LVMI).

GROSS MORPHOLOGY. The heart was excised from the chest cavity, the excess blood was flushed out from the chambers, and then the heart was weighed. The heart weight was indexed to body weight and the mean values compared among the groups.

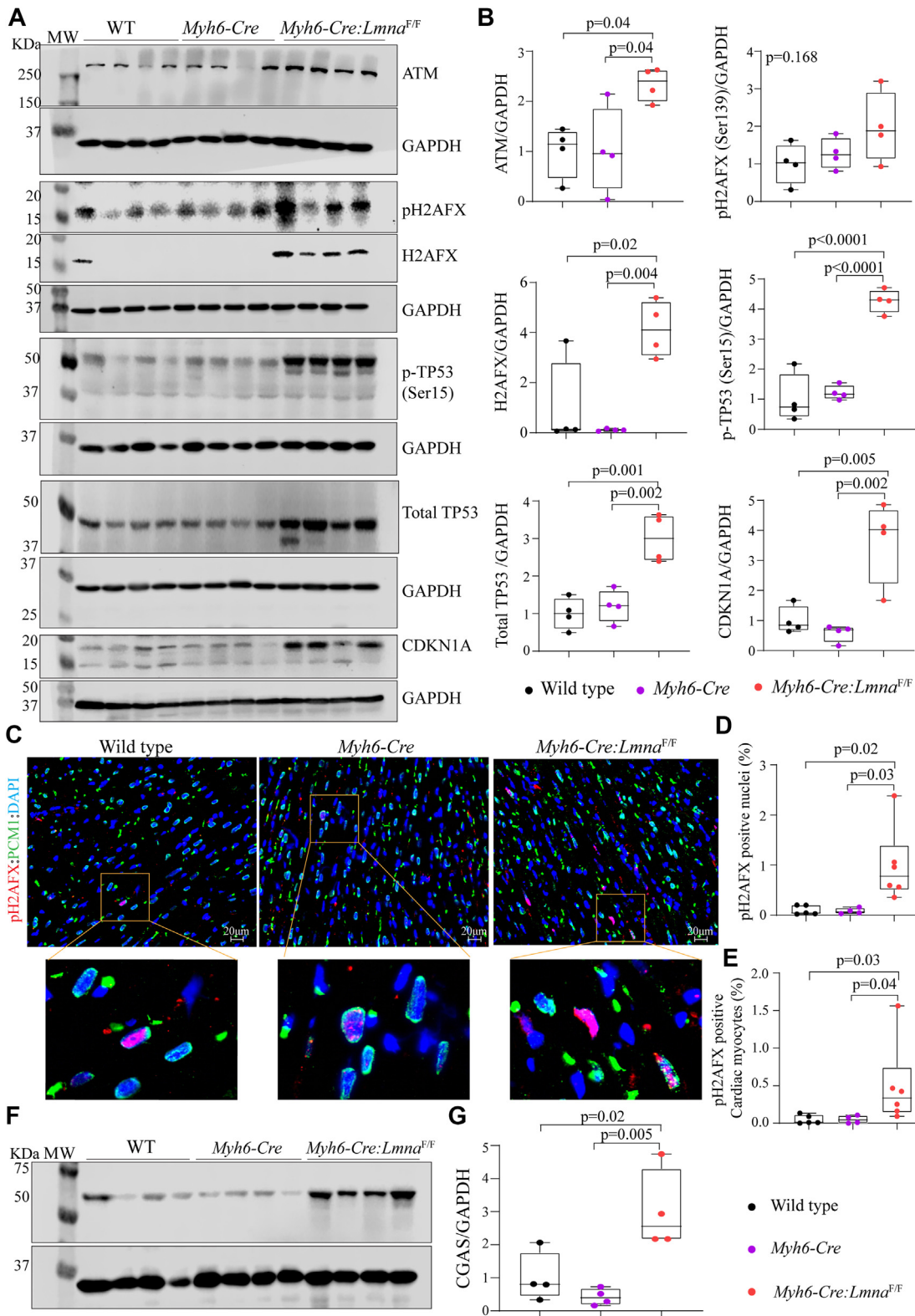
IMMUNOBLOTTING. Expression of the selected proteins in the mouse heart was analyzed by means of immunoblotting, as published.^{17,22} Briefly, the heart tissue was minced and homogenized in radioimmunoprecipitation buffer (Pierce, cat. no. 89900)

containing 25 mmol/L Tris-HCl pH 7.6, 150 mmol/L NaCl, 1% NP40, 1% sodium deoxycholate, and 0.5% sodium dodecyl sulfate as well as protease and phosphatase inhibitors (Roche cat #4693116001 and cat #49068459001). Protein extracts were quantified with the use of the Bradford protein assay reagent (ThermoFisher Scientific, cat. no. 23200) with a spectrophotometer at 595 nm wavelength. Aliquots of 50-75 μ g protein lysates were denatured, resolved on 8%-15% sodium dodecyl sulfate-polyacrylamide gel electrophoresis gel, and transferred onto a nitrocellulose membrane. The membranes were probed with antibodies to detect the target protein of interest specified in [Supplemental Table 1](#). Immunoblotting was performed with all samples loaded into a single gel, and the signal intensities on a single blot were compared to avoid drift in data quantification.

IMMUNOFLUORESCENCE. Expression and localization of pH2AFX were detected by immunofluorescence staining of thin myocardial sections, as published.^{15,22,25} Briefly, the hearts were placed on an Optimal cutting temperature compound (OCT) (Fisher, cat. no. 23-730-571) and snap-frozen in cold 2-methyl butane. Thin 5- μ m myocardial sections were obtained by sectioning using a cryostat and fixed in 4% formaldehyde at room temperature for 10 minutes. The myocardial sections were incubated in a blocking buffer containing 10% goat serum and 1% bovine serum albumin in 1 \times phosphate-buffered saline solution (PBS) containing 0.5% Triton X-100 followed by overnight incubation at 4 °C with the antibody against pH2AFX, as specified in [Supplemental Table 1](#). Following incubation with the primary antibody, sections were then incubated with a secondary antibody conjugated with a fluorescent dye. Nuclei were counterstained with 4',6-diamidino-2-phenylindole dihydrochloride (DAPI) (Sigma-Aldrich, cat. no. D8417). The sections were mounted with fluorescent mounting medium (Dako, cat. no. S3023) and imaged with an inverted fluorescent microscope (Axioplan Fluorescence Microscope, Zeiss) using AxioVision software. Quantitation was performed in at least 30 images of \times 40 magnification field from a minimum of 3-6 sections and at least 5 animals in each experimental group. A total of 8,000-15,000 DAPI-positive nuclei were counted per animal. Images were analyzed with the use of Image J software.

MYOCARDIAL FIBROSIS. Mice were killed by CO₂ inhalation followed by cervical dislocation. Hearts were removed from the chest cavity, rinsed in cold PBS, and fixed overnight in 10% neutral-buffered formalin. The heart tissue was dehydrated in a

FIGURE 1 Activation of the DDR Pathway in the *Myh6-Cre:Lnna^{F/F}* Mouse Hearts



Continued on the next page

gradient of ethanol concentrations of 70%, 80%, 95%, and 100% followed by incubation in xylene for 15 minutes 2 times and embedded in paraffin. Thin myocardial sections were cut using a microtome (Leica) and placed on top of a Superfrost microscopic slide (VWR, cat. no. 48311-703).

Cardiac fibrosis was detected in the myocardial sections by staining in Picosirius red as published.^{15,21} Thin myocardial sections were deparaffinized in xylene for 15 minutes 2 times and rehydrated in 100%, 95%, 80%, 70%, and 50% ethanol gradient for 2 minutes each. The slides were washed in water and incubated with Picosirius red staining solution (Sigma Aldrich, cat. no. P6744-1GA) according to the manufacturer's instructions. Images were acquired with the use of an Olympus BX40 microscope equipped with a digital camera. Image J software was used to calculate collagen volume fraction (CVF) by analyzing 10 high-magnification fields ($\times 20$) per section and in 6 sections per heart and at least 5 mice per genotype.

MYOCARDIAL APOPTOSIS. Myocardial apoptosis was detected using a terminal deoxynucleotide transferase-mediated dUTP nick-end labeling (TUNEL) assay and In-Situ Cell Death Detection Fluorescein Kit (Roche, cat no. 11684795910) as published.^{15,17,21-23} Briefly, the myocardial sections were deparaffinized in xylene for 15 minutes 2 times followed by rehydration in ethanol gradient as described above. After washing in PBS, the sections were treated with proteinase K at a concentration of 20 $\mu\text{g}/\text{mL}$ in 10 mmol/L Tris-HCl pH 7.5 buffer containing 1 mg/mL bovine serum albumin for 20 minutes at room temperature. After the proteinase K treatment, the sections were washed in PBS and incubated with TUNEL reaction mixture for 1 hour at 37 °C, and nuclei

were counterstained with 1 $\mu\text{g}/\text{mL}$ DAPI. Images were acquired by means of a Zeiss Axioplan fluorescence microscope using Axiovision software. A total of 30 high-magnification fields representing 6 sections per heart and at least 5-7 mice per group were analyzed with the use of Image J software to calculate the percentage of nuclei that stained positive for the TUNEL assay. A total of 20,000-40,000 DAPI-positive nuclei were counted per heart and the mean percentages of TUNEL-positive nuclei were compared among the genotypes.

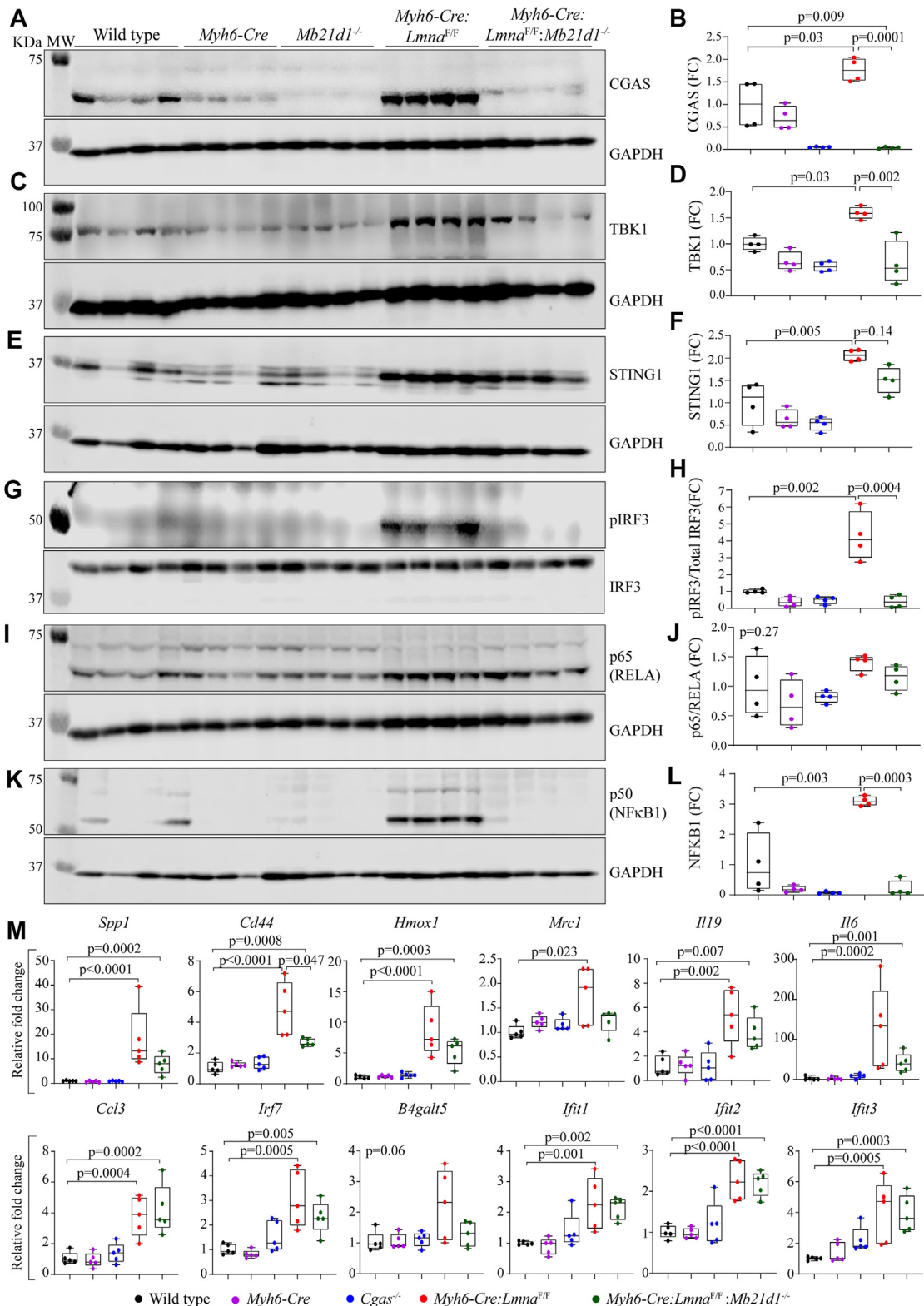
REVERSE-TRANSCRIPTION PCR. Total RNA was isolated from the heart tissue with the use of miRNeasy Mini Kit (Qiagen, cat. no. 217006) following the manufacturer's instructions. The genomic DNA was removed with the use of DNase I (Qiagen, cat. no. 79254) by in-column digestion. Around 1 μg total RNA was reverse transcribed with the use of a high-capacity cDNA synthesis kit (Applied Biosystems, cat. no. 4368814) and random primers. Approximately 5 ng cDNA was used to determine the transcript levels using either Sybr green or TaqMan assay reagents. Changes in the transcript levels were calculated with the use of the $\Delta\Delta\text{Ct}$ method. *Gapdh* transcript levels were used to normalize the transcript levels of genes of interest. The relative fold changes were presented by normalizing to the WT transcript levels. All reverse-transcription (RT) PCR experiments were conducted in technical duplicates and 5 biological replicates. Primers used in the study are presented in the [Supplemental Table 1](#).

STATISTICAL METHODS. An equal number of male and female mice were used in all of the experiments. Data analysis was performed without the knowledge of genotype wherever possible. Only 1 mouse per

FIGURE 1 Continued

(A) Immunoblot analysis showing expression of key proteins involved in the DDR pathway, including ATM, pH2AFX, H2AFX, phosphorylated P53 (Ser15), total P53, and CDKN1A, the latter a bona fide target of the TP53, in the whole heart extracts in the 3-week-old wild-type (WT), *Myh6-Cre*, and *Myh6-Cre:Lmna^{F/F}* mice. (B) Quantitative data depicting expression levels of the key DNA damage response proteins. Data are normalized to the corresponding GAPDH protein levels and presented as fold change relative to the expression levels in WT mice. (C) Representative immunofluorescence panels of thin myocardial sections, including magnified views, from the 3-week-old WT, *Myh6-Cre*, and *Myh6-Cre:Lmna^{F/F}* mice stained for the expression of phosphorylated H2AFX (Ser139), a marker of double-stranded DNA breaks. The pH2AFX protein is shown in red and PCMI, which tags the cardiac myocyte nuclei, is shown in green. Nuclei are counterstained with DAPI. (D, E) Quantitative data showing (D) percentage of the nuclei expressing pH2AFX in the whole myocardium and (E) percentage of cardiac myocyte nuclei costained for pH2AFX and PCMI. A total of 8,000-20,000 DAPI-stained nuclei were counted per heart and in a total of 4-6 hearts per genotype. The data are presented as percentage of nuclei stained for the marker of interest. (F) Immunoblot showing increased levels of the cyclic GMP-AMP synthase (CGAS) protein in the hearts of *Myh6-Cre:Lmna^{F/F}* mice compared with the WT and *Myh6-Cre* control mouse hearts at 3 weeks of age. (G) Quantitative data depicting CGAS protein expression levels in the WT, *Myh6-Cre*, and *Myh6-Cre:Lmna^{F/F}* mouse hearts. In all figures, the normally distributed data among the groups were compared by means of 1-way analysis of variance followed by Bonferroni pairwise multiple comparisons test. Otherwise, data were analyzed by means of Kruskal-Wallis test followed by Dunn multiple comparisons test (D and E). Only significant *P* values are presented. In all graphs, each dot represents 1 independent sample.

FIGURE 2 Genetic Blockade of the DDR Pathway in the *Myh6-Cre:Lmna^{F/F}* Mice



Continued on the next page

litter was randomly selected and used in the molecular biology and histology experiments to maintain the assumption of independence of the samples in the statistical analysis. However, multiple mice from the same litter were included in the survival analysis and the echocardiographic assessment of cardiac function. This approach might induce correlation between mice in each genotype. Because it was not feasible to identify the litter structure, survival analysis and echocardiographic data were analyzed on the assumption of independence.

The data were analyzed for gaussian distribution by means of the Shapiro-Wilk normality test. An α value of >0.05 was set as an indication of non-departure from normality. The data that followed normal distribution were analyzed by means of 1-way analysis of variance followed by Bonferroni pairwise multiple comparisons test. The main experimental groups, namely, the WT, *Myh6-Cre:Lnna^{F/F}*, and *Myh6-Cre:Lnna^{F/F}:Mb21d1^{-/-}* mice were included in the statistical analysis. The data deviating from the gaussian distribution were analyzed by means of Kruskal-Wallis test followed by Dunn correction for multiple comparisons. The average ratios of the signal intensity in the test to loading control protein were compared among the groups. The Ct values of the technical replicates were averaged and used to calculate the Δ Ct values between each test and control gene in the RT-PCR experiments. The Δ Ct values were used in the statistical analyses. The $\Delta\Delta$ Ct values were used to show the fold change in the graphic data presentation.

The survival rates between *Myh6-Cre:Lnna^{F/F}* and *Myh6-Cre:Lnna^{F/F}:Mb21d1^{-/-}* mice were analyzed by

means of the log-rank test. Each vertical drop in the survival curves indicates an event (death), and each dot represents the censoring age of a mouse alive at the time of data analysis. Mice were killed when in the moribund state, as determined by the institution care-providing veterinarian, or died naturally. Categorical values were analyzed by means of Fisher exact or chi-square test. All of the data were presented as mean \pm SD. Statistical analysis was performed in GraphPad Prism 8.0.

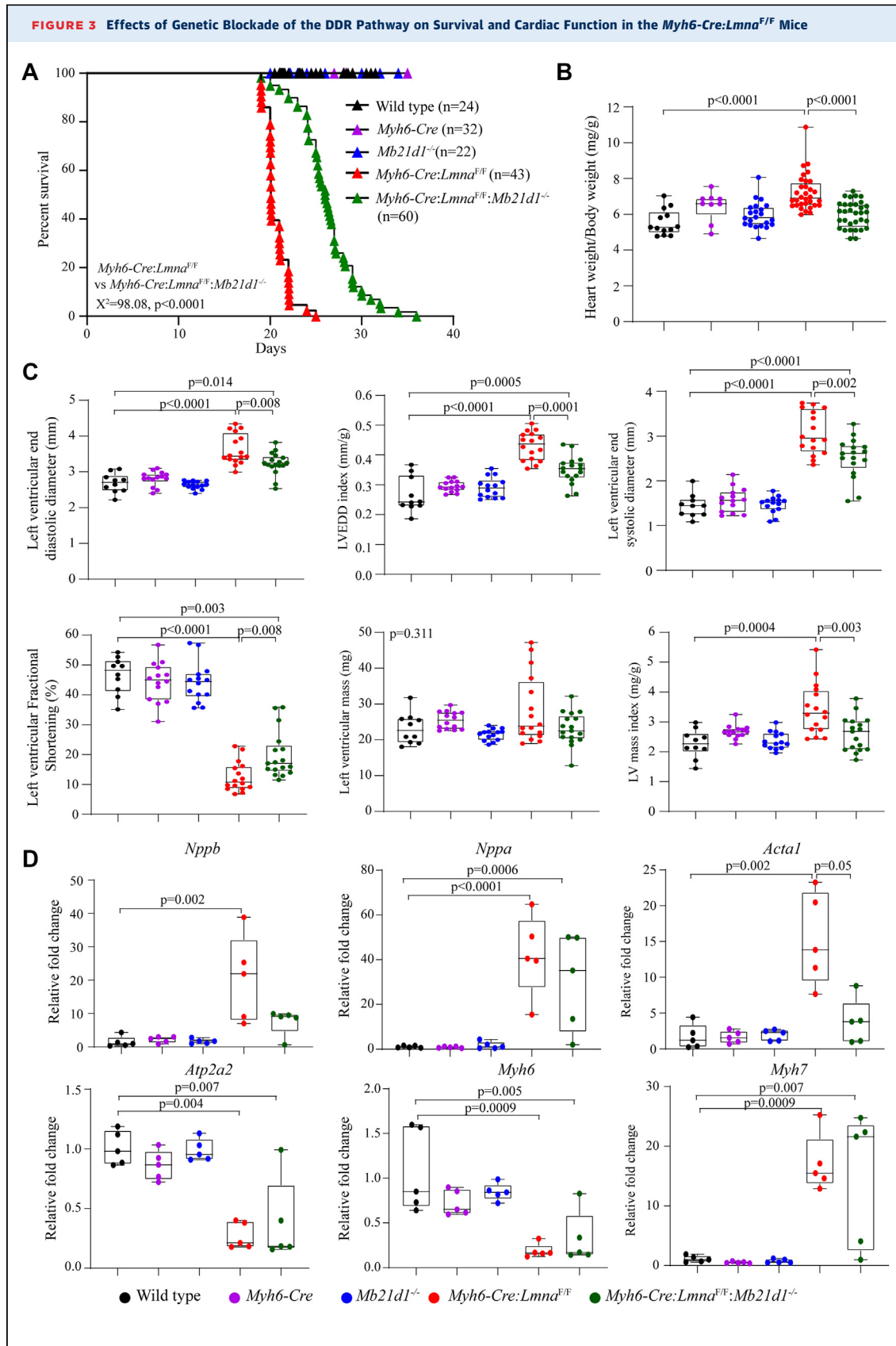
STUDY APPROVAL. Animal procedures complied with the National Institutes of Health Guidelines for the Care and Use of Laboratory Animals and were approved by the Animal Care and Use Committee of the University of Texas Health Science Center-Houston (AWC-21-0015).

RESULTS

ACTIVATION OF THE DDR PATHWAY IN THE *Myh6-Cre:Lnna^{F/F}* MOUSE HEARTS. To assess activation of the DDR pathway, levels of key DDR pathway proteins were determined with the use of immunoblotting in the cardiac protein extracts. Levels of ATM, H2AFX, P(Ser15)TP53, total TP53, and CDKN1A were markedly increased in the *Myh6-Cre:Lnna^{F/F}* compared with the *Myh6-Cre* or WT mouse hearts (Figures 1A and 1B). The *Lnna^{F/F}* mice were not included in the studies, because they do not exhibit a discernible phenotype.¹⁷ To test for corroboration of the findings, thin myocardial sections were co-immunostained for the expression of pH2AFX and pericentriolar membrane 1 protein, the latter to mark the cardiac myocyte nuclei.^{8,26} The number of

FIGURE 2 Continued

(A) Immunoblots and (B) quantitative data showing increased expression levels of the CGAS protein in the whole heart protein lysates from the *Myh6-Cre:Lnna^{F/F}* mice and complete absence of the cyclic GMP-AMP synthase (CGAS) protein in *Mb21d1^{-/-}* mouse hearts and its marked reduction in the *Myh6-Cre:Lnna^{F/F}:Mb21d1^{-/-}* mouse hearts. (C) Immunoblots and (D) quantitative data showing increased expression levels of the TBK1 in the whole heart protein lysates from the *Myh6-Cre:Lnna^{F/F}* mice and its reduction on deletion of the *Mb21d1* gene in the *Myh6-Cre:Lnna^{F/F}:Mb21d1^{-/-}* hearts. (E) Immunoblots and (F) quantitative data showing expression levels of the STING1 protein, a downstream target of CGAS, in the whole heart lysates from the wild-type, *Myh6-Cre*, *Mb21d1^{-/-}*, *Myh6-Cre:Lnna^{F/F}*, and *Myh6-Cre:Lnna^{F/F}:Mb21d1^{-/-}* mice. (G) Immunoblots and (H) quantitative data showing comparisons of the expression of (top) pIRF3 and (bottom) total IRF3 in the 5 genotypes. Data show marked elevation of pIRF3 levels in the *Myh6-Cre:Lnna^{F/F}* mouse hearts and normalization of the levels on deletion of *Mb21d1* gene. (I, K) Immunoblots and (J, L) quantitative data showing expression levels of components of the canonic NF κ B pathway, including (I, J) RELA/p65 and (K, L) NF κ B1/P50 in the wild-type, *Myh6-Cre*, *Mb21d1^{-/-}*, *Myh6-Cre:Lnna^{F/F}*, and *Myh6-Cre:Lnna^{F/F}:Mb21d1^{-/-}* mouse hearts. (M) Transcript levels of selected targets of NF κ B and IRF3 transcription factors, as quantified by reverse-transcription polymerase chain reaction. Transcript levels of selected but not all targets show increased levels in the *Myh6-Cre:Lnna^{F/F}* mouse hearts and their attenuation in the *Myh6-Cre:Lnna^{F/F}:Mb21d1^{-/-}* mouse hearts. The wild-type, *Myh6-Cre*, and *Mb21d1^{-/-}* mouse hearts were included as control groups. Δ Ct values were used to calculate *P* values by means of 1-way analysis of variance (ANOVA) comparing wild-type, *Myh6-Cre:Lnna^{F/F}*, and *Myh6-Cre:Lnna^{F/F}:Mb21d1^{-/-}* genotypes. Only the significant *P* values were presented. Some of the membranes were stripped and re-probed with different antibodies. Therefore, the same membranes were also re-probed with the antibody against GAPDH. Only significant *P* values are presented after comparing the 3 main groups, that is, wild-type, *Myh6-Cre:Lnna^{F/F}*, and *Myh6-Cre:Lnna^{F/F}:Mb21d1^{-/-}*, by means of 1-way ANOVA followed by Bonferroni pairwise multiple comparisons test.



Continued on the next page

myocytes expressing pH2AFX was increased in the *Myh6-Cre:Lnna^{F/F}* mouse hearts, representing approximately 0.49% ± 0.54% of the myocyte nuclei (Figures 1C to 1E). Finally, levels of CGAS protein, the cytosolic DNA sensor, were assessed with the use of immunoblotting, and they were markedly increased in the *Myh6-Cre:Lnna^{F/F}* mouse hearts (Figures 1F and 1G).

GENETIC ABLATION OF THE *Mb21d1* GENE IN THE *Myh6-Cre:Lnna^{F/F}* MOUSE HEARTS. To block the CGAS component of the DDR pathway, *Myh6-Cre:Lnna^{F/F}* mice were crossed with the *Mb21d1* knockout mice. To test effective blockade of the CGAS pathway, expression of the CGAS protein, encoded by the *Mb21d1* gene, and its downstream effectors were analyzed with the use of immunoblotting. The CGAS protein was expressed at low levels in the WT and *Myh6-Cre* mouse hearts, its expression was not detected in the *Mb21d1^{-/-}* mouse heart, as expected, and its levels were markedly increased in the *Myh6-Lmna^{F/F}* mouse hearts (Figures 2A and 2B).

GENETIC BLOCKADE OF THE CGAS PATHWAY. Deletion of the *Mb21d1* gene in the *Myh6-Lmna^{F/F}* mouse hearts abolished expression of the CGAS protein (Figures 2A and 2B). Likewise, whereas levels of TBK1 and STING1 were increased in the *Myh6-Lmna^{F/F}* mouse hearts, in the *Myh6-Cre:Lnna^{F/F}:Mb21d1^{-/-}* mouse hearts, TBK1 levels were reduced to levels similarly to those in the WT and *Myh6-Cre* control mouse hearts, whereas the reduction in STING1 levels were modest (Figures 2C to 2F).

The TBK1-STING1 complex targets IRF3 for activation by phosphorylation and activation of the canonic (p65 and p50) and noncanonic (p52 and RELB) components of the NFκB1 pathway. Immunoblotting showed increased pIRF3 levels in the *Myh6-Lmna^{F/F}* mouse hearts and normalization of the levels in *Myh6-Cre:Lnna^{F/F}:Mb21d1^{-/-}* mouse hearts (Figures 2G and 2H). Changes in the p65 (RELA) components of the NFκB1 pathway were less remarkable (Figures 2I and 2J), whereas levels of p50 (NFκB1), which were

increased in the *Myh6-Lmna^{F/F}* mouse hearts, were normalized in the *Myh6-Cre:Lnna^{F/F}:Mb21d1^{-/-}* mouse hearts (Figures 2K and 2L).

To further assess inhibition of the CGAS pathway, transcript levels of selected genes that are known to be targets of IRF3 and NFκB1 were analyzed with the use of RT-PCR. Transcript levels of several but not all tested NFκB and IRF3 target genes were increased in the *Myh6-Cre:Lnna^{F/F}* mouse hearts (Figure 2M). Deletion of the *Mb21d1* gene attenuated transcript levels of several IRF3 and NFκB1 target genes in the *Myh6-Cre:Lnna^{F/F}:Mb21d1^{-/-}* mouse hearts, but only the *Cd44* transcript levels were reduced significantly (Figure 2M).

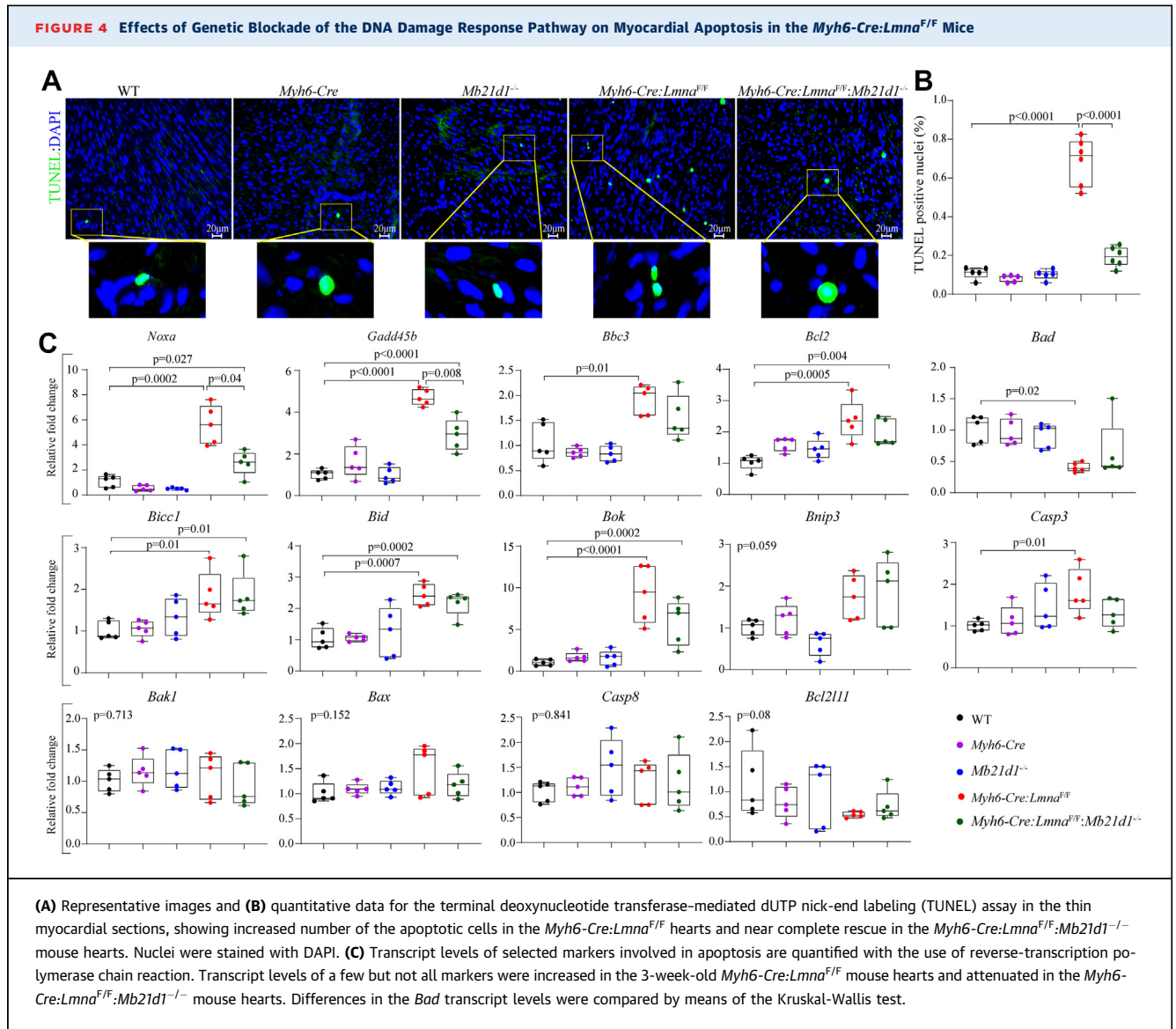
PHENOTYPIC CONSEQUENCES OF GENETIC BLOCKADE OF CGAS PATHWAY IN THE *Myh6-Cre:Lnna^{F/F}* MICE. The *Mb21d1^{-/-}* mice showed no discernible cardiac phenotype during the time course of the study, which is consistent with the initial description of this genetic model.²⁰ However, deletion of the *Mb21d1* gene significantly attenuated the cardiac phenotype in the *Myh6-Cre:Lnna^{F/F}* mice.

Survival. The WT, *Myh6-Cre*, and *Mb21d1^{-/-}* mice had normal survival, but, as reported previously, the *Myh6-Cre:Lnna^{F/F}* mice exhibit total mortality within the first 4 weeks of life with maximum and median survival rates of 25 and 20 days, respectively (Figure 3A).¹⁷ Deletion of the *Mb21d1* gene prolonged the maximum and median survival rates of the *Myh6-Cre:Lnna^{F/F}* mice to 36 and 26 days, respectively (Figure 3A).

Cardiac size and function. Heart weight-body weight ratio was increased in the *Myh6-Cre:Lnna^{F/F}* compared with the WT, *Myh6-Cre*, and *Mb21d1^{-/-}* mice, whereas it was similar between the WT, *Myh6-Cre*, and *Myh6-Cre:Lnna^{F/F}:Mb21d1^{-/-}* mice (Figure 3B). Evaluation of cardiac size and function by means of echocardiography showed markedly increased LVEDD and LVESD and reduced LVFS in the *Myh6-Cre:Lnna^{F/F}* mice (Figure 3C, Table 1). Deletion of *Mb21d1* significantly attenuated the

FIGURE 3 Continued

(A) Kaplan-Meier survival plots showing the survival rates in the wild-type, *Myh6-Cre*, *Mb21d1^{-/-}*, *Myh6-Cre:Lnna^{F/F}*, and *Myh6-Cre:Lnna^{F/F}:Mb21d1^{-/-}* mice. The log-rank test was used to calculate chi-square and *P* values. Each vertical drop in the survival curves indicates an event (death) and each dot represents the censoring age of a mouse alive at the time of data analysis. (B) Graph depicting the increased heart weight to body weight ratio in the 3-week-old *Myh6-Cre:Lnna^{F/F}* mice compared with wild-type and normalization of the ratio in the *Myh6-Cre:Lnna^{F/F}:Mb21d1^{-/-}* mice. (C) Selected echocardiographic indices of cardiac size and function in the 5 genotypes showing increased cardiac size and depressed function in the *Myh6-Cre:Lnna^{F/F}* mice and attenuation of the indices in the *Myh6-Cre:Lnna^{F/F}:Mb21d1^{-/-}* mice. (D) Transcript levels of selected markers of cardiac dysfunction in 3-week-old mice as assessed with the use of reverse-transcription polymerase chain reaction, showing the anticipated dysregulation in the *Myh6-Cre:Lnna^{F/F}* hearts and their attenuation in *Myh6-Cre:Lnna^{F/F}:Mb21d1^{-/-}* hearts. LV = left ventricular; LVEDD = left ventricular end-diastolic diameter.



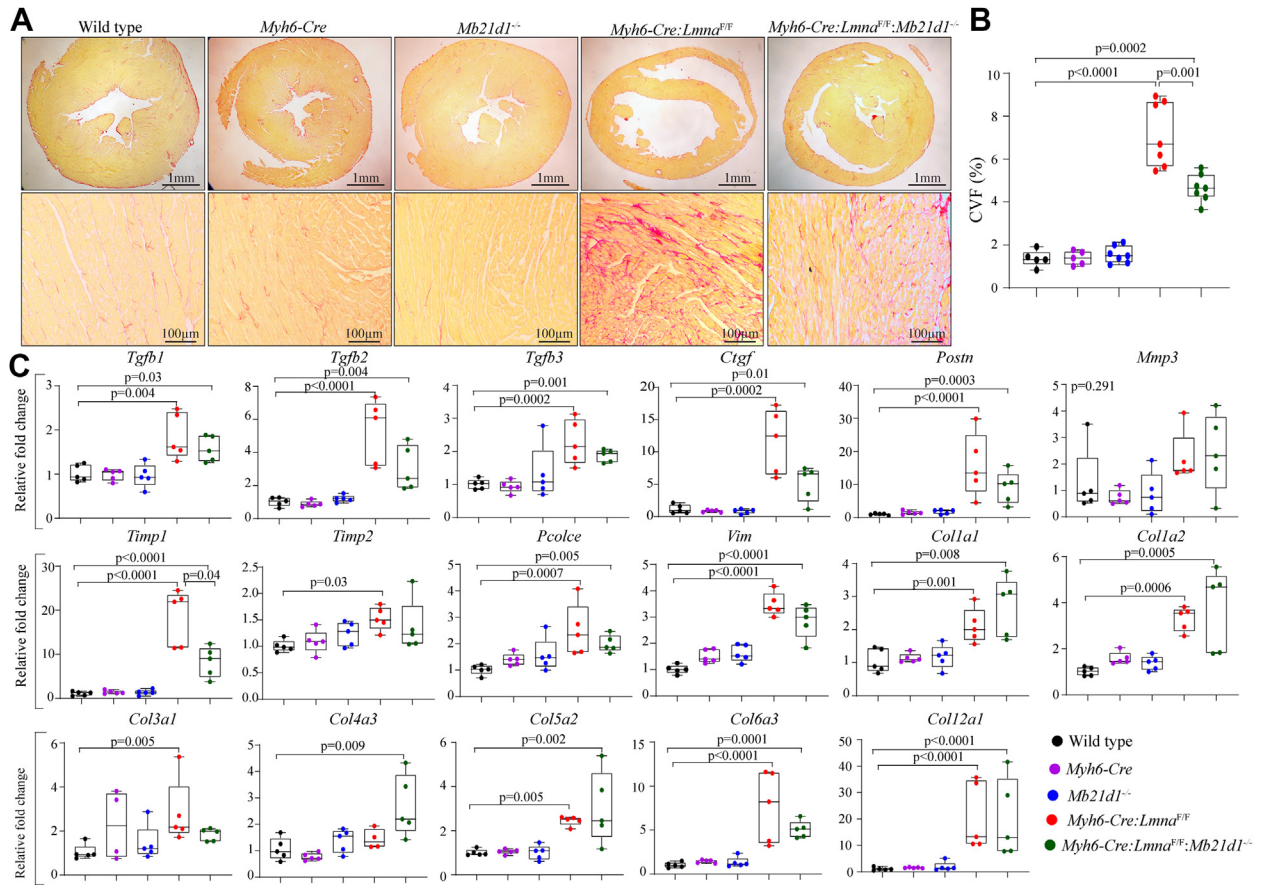
cardiac phenotype by improving LVEDD, LVESD, and LVFS in the *Myh6-Cre:Lnna^{F/F}* mice (Figure 3C, Table 1).

In accord with improved indices of cardiac size and function, deletion of *Mb21d1* also improved transcript levels of markers of cardiac hypertrophy and failure in the *Myh6-Cre:Lnna^{F/F}* mice (Figure 3D). Accordingly, transcript levels of *Nppb*, *Nppa*, *Acta1*, and *Myh7* were increased in the myocardium from the *Myh6-Cre:Lnna^{F/F}* mice, whereas levels of *Atp2a2* and *Myh6* were reduced, all of which are consistent with the molecular phenotype of heart failure (Figure 3D). Deletion of *Mb21d1* reversed and attenuated transcript levels of *Nppb*, *Nppa*, and *Acta1*, markers of cardiac hypertrophy and failure, but only

Acta1 transcript levels met the statistical significance level (Figure 3D).

Myocardial apoptosis. Myocardial apoptosis was assessed with the use of the TUNEL assay as well as quantification of transcript levels of selected genes involved in apoptosis. The number of nuclei that stained positive for the TUNEL assay was markedly increased in the *Myh6-Cre:Lnna^{F/F}* mouse myocardium, whereas the number of apoptotic nuclei was reduced in the *Myh6-Cre:Lnna^{F/F};Mb21d1^{-/-}* mouse myocardium (Figures 4A and 4B). In accord with the increased number of the TUNEL-positive nuclei, transcript levels of several genes involved in apoptosis had changed in the *Myh6-Cre:Lnna^{F/F}* mouse myocardium (Figure 4C). Deletion of the

FIGURE 5 Effects of Genetic Blockade of the DNA Damage Response Pathway on Myocardial Fibrosis in the *Myh6-Cre:Lnna^{F/F}* Mice



(A) Representative images of thin myocardial sections stained with Picrosirius red in the 5 experimental groups. **(Top)** Low- and **(bottom)** high-magnification panels are shown. **(B)** Quantitative data depicting collagen volume fraction (CVF) in the experimental groups. CVF was markedly increased in the 3 weeks old *Myh6-Cre:Lnna^{F/F}* mouse hearts and reduced in the *Myh6-Cre:Lnna^{F/F}:Mb21d1^{-/-}* mouse hearts. **(C)** Transcript levels of selected markers involved in fibrosis as quantified with the use of reverse-transcription polymerase chain reaction. The data show increased transcript levels of selected but not all markers in the 3-week-old *Myh6-Cre:Lnna^{F/F}* hearts compared with control groups and their attenuation in the *Myh6-Cre:Lnna^{F/F}:Mb21d1^{-/-}* mouse hearts.

Mb21d1 gene reduced transcript levels of *Noxa* and *Gadd45b* genes (Figure 4C).

Myocardial fibrosis. Fibrosis was assessed by quantification of CVF on staining of the thin myocardial section with Picrosirius red, which constituted about 7.2% of the myocardium in the *Myh6-Cre:Lnna^{F/F}* mouse myocardium, compared with around 1% in the WT, *Myh6-Cre*, and *Mb21d1^{-/-}* mice (Figures 5A and 5B). CVF was significantly attenuated in the *Myh6-Cre:Lnna^{F/F}:Mb21d1^{-/-}* mouse myocardium. Likewise, RT-PCR analysis of transcript levels of several genes involved in fibrosis showed increased levels in the *Myh6-Cre:Lnna^{F/F}* mouse myocardium and attenuation of the transcript levels of several genes in the *Myh6-Cre:Lnna^{F/F}:Mb21d1^{-/-}* mice, however, the attenuation met the

criterion for statistical significance only for the *Timp1* gene (Figure 5C).

DISCUSSION

The findings of this study highlight significant contributions of DSBs and activation of the CGAS axis of the DDR pathways to the pathogenesis of DCM caused by LMNA deficiency. The DDR pathway is activated in the *Myh6-Cre:Lnna^{F/F}* mouse hearts, and genetic blockade of the CGAS component of the DDR pathway, on deletion of the *Mb21d1* gene, which encodes the CGAS protein, improved survival and cardiac function, and attenuated myocardial fibrosis and apoptosis. CGAS is the best characterized as a cytosolic DNA sensor, which on binding to the

TABLE 1 Echocardiographic Indices of Cardiac Size and Function

	WT (n = 10)	Myh6-Cre (n = 14)	Mb21d1 ^{-/-} (n = 14)	Myh6-Cre:Lnma ^{F/F} (n = 16)	Myh6-Cre:Lnma ^{F/F} : Mb21d1 ^{-/-} (n = 17)	P Value
Male/female	5/5	6/8	4/10	6/10	9/8	0.687
Age, d	20.10 ± 0.88	20.86 ± 1.46	20.43 ± 1.34	20.38 ± 0.89	20.06 ± 1.25	0.237 ^a
Body weight, g	10.59 ± 2.58	9.55 ± 0.62	9.14 ± 0.85	8.21 ± 1.18 ^{b,c}	9.02 ± 1.31	0.009 ^a
Heart rate, beats/min	496.18 ± 16.43	501.16 ± 23.46	508.47 ± 16.22	479.51 ± 36.75	498.45 ± 31.43	0.094
IVST, mm	0.46 ± 0.04	0.45 ± 0.03	0.44 ± 0.03	0.37 ± 0.03 ^{b,c,d}	0.36 ± 0.03 ^{b,c,d}	<0.0001
PWT, mm	0.47 ± 0.04	0.49 ± 0.05	0.46 ± 0.04	0.37 ± 0.05 ^{b,c,d}	0.39 ± 0.04 ^{b,c,d}	<0.0001
LVEDD, mm	2.69 ± 0.27	2.81 ± 0.20	2.63 ± 0.11	3.50 ± 0.42 ^{b,c,d}	3.11 ± 0.31 ^{b,d,e}	<0.0001
LVEDDI, mm/g	0.27 ± 0.06	0.29 ± 0.02	0.29 ± 0.03	0.43 ± 0.05 ^{b,c,d}	0.35 ± 0.05 ^{b,c,d,e}	<0.0001
LVEDS, mm	1.44 ± 0.26	1.57 ± 0.27	1.47 ± 0.19	3.07 ± 0.48 ^{b,c,d}	2.51 ± 0.45 ^{b,c,d,e}	<0.0001
FS, %	46.58 ± 6.18	44.40 ± 6.67	44.19 ± 6.73	12.54 ± 4.97 ^{b,c,d}	19.81 ± 7.74 ^{b,c,d,e}	<0.0001
LVM, mg	23.19 ± 4.30	25.51 ± 2.43	21.49 ± 1.61 ^c	28.41 ± 9.50	23.15 ± 4.51	0.014 ^a
LVMI, mg/g	2.27 ± 0.47	2.67 ± 0.23	2.37 ± 0.29	3.43 ± 0.85 ^{b,d}	2.60 ± 0.57 ^e	0.0002

Values are mean ± SD. Chi-square test was used to assess the M/F distribution, and normally distributed samples were analyzed by means of 1-way analysis of variance with Bonferroni pairwise comparisons. ^aP value determined by means of Kruskal-Wallis test with Dunn test for multiple comparisons. ^bSignificant P value compared with wild type. ^cSignificant P value compared with *Myh6-Cre*. ^dSignificant P value compared with *Mb21d1^{-/-}*. ^eSignificant P value compared with *Myh6-Cre:Lnma^{F/F}*.

IVST = interventricular septal thickness; LVEDD = left ventricular end-diastolic diameter; LVEDDI = left ventricular end diastolic diameter index; LVEDS = left ventricular end systolic diameter; LVFS = left ventricular fractional shortening; LVM = left ventricular mass; LVMI = left ventricular mass index; M/F = male/female; PWT = posterior wall thickness; WT = wild type.

cytosolic DNA activates the TBK1-STING1 complex, leading to increased transcriptional activities of the IRF3 and NFκB pathway and consequent expression of the proinflammatory cytokines. Several components of the CGAS pathway were activated in *Myh6-Cre:Lnma^{F/F}* mouse hearts, including CGAS, TBK1, and STING1 proteins and their downstream effectors of gene expression pIRF3 and NFκB transcriptional regulators. Similarly, increased expression of mitotic factors, such as transforming growth factor β1, likely as part of the senescence-associated secretory phenotype, provides a mechanistic explanation for increased myocardial fibrosis in the *Myh6-Cre:Lnma^{F/F}* mouse myocardium. Genetic ablation of the *Mb21d1* gene normalized elevated levels of the CGAS pathway proteins and suppressed expression of the proinflammatory cytokines through pIRF3 and NFκB pathways, providing a mechanistic basis for the salutary effects of genetic blockade of the CGAS/DDR pathway in this mouse model of LMNA-associated DCM.

Activation of the DDR pathway in the *Myh6-Cre:Lnma^{F/F}* mouse hearts was confirmed for multiple components of the pathway and by complementary methods. The beneficial effects of genetic blockade of the CGAS pathway were consistent across the clinical (survival), functional (echocardiographic phenotype), histologic (fibrosis and apoptosis), and molecular (gene expression) phenotypes and were mostly confirmed by alternative methods. Likewise, the effect sizes of the beneficial effects, such as a 30% improvement in survival, were notable and beyond the biological variability that is often observed in the

model organisms. The findings of the genetic ablation of the CGAS pathway provide proof-of-principle data and set the stage for follow-up pharmacologic inhibition of this pathway for therapeutic gains in DCM observed in laminopathies. Given that CGAS and the DDR pathways are implicated in other forms of inherited cardiomyopathies as well as in heart failure in general, the findings might have broader clinical implications.^{22,27} Small molecule inhibitors of the CGAS pathway protein have been developed and are currently being tested for their efficacy in various pathologic conditions.^{28,29}

The phenotype rescue, not unexpectedly, was incomplete, which is in accord with the multifarity of the involved mechanisms in the pathogenesis of DCM caused by LMNA deficiency. A notable example is the ATM/TP53 component of the DDR pathway, which was activated in the *Myh6-Cre:Lnma^{F/F}* mice. Activation of the ATM/TP53 pathway in response to DSBs is mostly independent from and in parallel to the activation of CGAS-TBK1-STING1 axis. Therefore, genetic deletion of the *Mb21d1* is not expected to directly target the ATM/TP53 and other dysregulated pathways, which could play major roles in the pathogenesis of the phenotype. It is also noteworthy that the deletion of the *Mb21d1* gene did not fully rescue all components of the NFκB pathway and expression levels of the proinflammatory cytokines that were analyzed in this study. The incomplete molecular rescue is also in agreement with regulation of expression of these key molecules through mechanisms independent of the CGAS-TBK1-STING1 axis.

By design, this was a preventive study, because the *Mb21d1*^{-/-} mice carry the germline deletion of the *Mb21d1* gene and therefore the CGAS protein was absent in the *Myh6-Cre:Lnna*^{F/F}:*Mb21d1*^{-/-} mice before the onset of heart failure. Whether inhibition of the CGAS protein would attenuate or reverse established heart failure in the *Myh6-Cre:Lnna*^{F/F} mice is an empirical question that awaits to be tested upon the development of a mouse model of inducible deletion of *Mb21d1*. Pharmacologic inhibition of CGAS, once pharmacokinetics and pharmacodynamics of the available CGAS inhibitors in mice are established, would enable testing of the effects of inhibition of CGAS on established heart failure. The use of the recombinant adeno-associated viruses to express a short hairpin RNA to knock down the expression of the *Mb21d1* gene would provide an alternative approach to testing the potential benefits of knocking down the CGS protein in heart failure.

Despite the evidence of activation of the CGAS molecule in various models of cardiac pathology, the relevance of the findings to human DCM caused by the *LMNA* mutations remains to be established.³⁰⁻³² Equally unclear is whether activation of CGAS is specific to heart failure caused by *LMNA* mutations or is generalizable to other forms of heart failure in humans. Given the cardinal role of the *LMNA* protein in genome stability, one might speculate that heart failure caused by *LMNA* mutations is the prime model for the activation of the CGAS pathway.^{33,34} Nevertheless, cell death and mitochondrial damage are common features of heart failure. Consequently, one might also envision the release of the genomic and/or mitochondrial DNA from the damaged myocardium, regardless of its cause, to activate the CGAS pathway in heart failure. Finally, whether increased expression of proinflammatory cytokines, ie, molecular inflammation, because of activation of the CGAS pathway also extends to cellular inflammation on recruitment of the inflammatory cells to the myocardium in heart failure caused by *LMNA* mutations should be tested.

The mechanisms involved in genomic instability in laminopathies, and therefore increased DSBs, are not well understood. The *LMNA* protein is implicated in the induction as well as the repair of the DNA breaks during replication stress.^{34,35} Accordingly, *LMNA* is considered to be necessary for the processing of topoisomerase 2B (TOP2B) at the chromatin loops, which cuts both DNA strands near the CTCF insulator to release the torsional stress and make the chromatin available for gene expression.^{36,37} Intact *LMNA*

function is considered necessary for the dissociation of TOP2B from the break sites and their repairs by the homologous recombination.³⁸⁻⁴⁰ Moreover, *LMNA* also interacts with several repair proteins and is considered to be essential for their recruitment to the DSB sites.⁴¹ Thus, in laminopathies both induction and repair of the DSBs might be affected.

In conclusion, the data showed activation of the DDR pathway, in response to DSBs, and the salubrious effects of genetic ablation of the *Mb21d1* gene, which encodes the key cytosolic DNA sensor CGAS, on multiple phenotypes in a mouse model of DCM caused by *LMNA* deficiency. The findings raise the prospect for pharmacologic interventions targeting the DDR pathway for therapeutic gains in DCM and possibly in other forms of heart failure.

FUNDING SUPPORT AND AUTHOR DISCLOSURES

Dr Cheedipudi is supported by a Career Development Grant from the American Heart Association (20CDA35310229). Ms Asghar has reported that she has no relationships relevant to the contents of this paper to disclose. Dr Marian is supported by the National Heart, Lung, and Blood Institute (HL151737, HL132401).

ADDRESS FOR CORRESPONDENCE: Dr Ali J. Marian, Center for Cardiovascular Genetics, 6770 Bertner Street, Suite C900A, Houston, Texas 77030, USA. E-mail: ali.j.marian@uth.tmc.edu.

PERSPECTIVES

COMPETENCY IN MEDICAL KNOWLEDGE: The findings of the present study inform clinicians and the researchers about the presence and clinical significance of DSBs and the cellular responses to DSBs in the pathogenesis of dilated cardiomyopathy.

TRANSLATIONAL OUTLOOK: The DDR pathway is activated in the heart in dilated cardiomyopathy caused by *LMNA* mutations. Activation of the DDR pathways provokes inflammatory responses contributing to myocardial fibrosis, cell death, and cardiac dysfunction. The findings of the present study, showing the beneficial effects of genetic inhibition of the DDR pathways in DCM, set the stage for the therapeutic targeting of the DDR pathway in heart failure. Pharmacologic inhibitors of the molecules involved in the DDR pathways are being tested in various diseases and are primed for testing for their beneficial effects in patients with heart failure.

REFERENCES

1. GBD 2017 Disease and Injury Incidence and Prevalence Collaborators. Global, regional, and national incidence, prevalence, and years lived with disability for 354 diseases and injuries for 195 countries and territories, 1990-2017: a systematic analysis for the Global Burden of Disease Study 2017. *Lancet*. 2018;392:1789-1858.
2. Emmons-Bell S, Johnson C, Roth G. *Prevalence, incidence and survival of heart failure: a systematic review*. *Heart*; 2022.
3. Khush KK, Cherikh WS, Chambers DC, et al. The International Thoracic Organ Transplant Registry of the International Society for Heart and Lung Transplantation: thirty-sixth adult heart transplantation report—2019; focus theme: donor and recipient size match. *J Heart Lung Transplant*. 2019;38:1056-1066.
4. Hershberger RE, Cowan J, Jordan E, Kinnamond DD. The complex and diverse genetic architecture of dilated cardiomyopathy. *Circ Res*. 2021;128:1514-1532.
5. Fatkin D, MacRae C, Sasaki T, et al. Missense mutations in the rod domain of the lamin A/C gene as causes of dilated cardiomyopathy and conduction-system disease. *N Engl J Med*. 1999;341:1715-1724.
6. Taylor MR, Fain PR, Sinagra G, et al. Natural history of dilated cardiomyopathy due to lamin A/C gene mutations. *J Am Coll Cardiol*. 2003;41:771-780.
7. Rober RA, Weber K, Osborn M. Differential timing of nuclear lamin A/C expression in the various organs of the mouse embryo and the young animal: a developmental study. *Development*. 1989;105:365-378.
8. Cheedipudi SM, Matkovich SJ, Coarfa C, et al. Genomic reorganization of lamin-associated domains in cardiac myocytes is associated with differential gene expression and DNA methylation in human dilated cardiomyopathy. *Circ Res*. 2019;124:1198-1213.
9. Coste Pradas J, Auguste G, Matkovich SJ, et al. Identification of genes and pathways regulated by lamin A in heart. *J Am Heart Assoc*. 2020;9:e015690.
10. Wong X, Stewart CL. The laminopathies and the insights they provide into the structural and functional organization of the nucleus. *Annu Rev Genomics Hum Genet*. 2020;21:263-288.
11. Worman HJ, Bonne G. "Laminopathies": a wide spectrum of human diseases. *Exp Cell Res*. 2007;313:2121-2133.
12. Perovanovic J, Dell'Orso S, Gnoch VF, et al. Laminopathies disrupt epigenomic developmental programs and cell fate. *Sci Transl Med*. 2016;8:335ra58.
13. De Vos WH, Houben F, Kamps M, et al. Repetitive disruptions of the nuclear envelope invoke temporary loss of cellular compartmentalization in laminopathies. *Hum Mol Genet*. 2011;20:4175-4186.
14. Cho S, Vashisth M, Abbas A, et al. Mechano-sensing by the lamina protects against nuclear rupture, DNA damage, and cell-cycle arrest. *Dev Cell*. 2019;49:920-935.e5.
15. Chen SN, Lombardi R, Karmouch J, et al. DNA damage response/TP53 pathway is activated and contributes to the pathogenesis of dilated cardiomyopathy associated with LMNA (lamin A/C) mutations. *Circ Res*. 2019;124:856-873.
16. Galluzzi L, Vanpouille-Box C, Bakhom SF, Demaria S. Snapshot: cGAS-STING signaling. *Cell*. 2018;173:276-276.e1.
17. Auguste G, Rouhi L, Matkovich SJ, et al. BET bromodomain inhibition attenuates cardiac phenotype in myocyte-specific lamin A/C-deficient mice. *J Clin Invest*. 2020;130:4740-4758.
18. Kim Y, Zheng Y. Generation and characterization of a conditional deletion allele for Lmna in mice. *Biochem Biophys Res Commun*. 2013;440:8-13.
19. Agah R, Frenkel PA, French BA, Michael LH, Overbeek PA, Schneider MD. Gene recombination in postmitotic cells. Targeted expression of Cre recombinase provokes cardiac-restricted, site-specific rearrangement in adult ventricular muscle in vivo. *J Clin Invest*. 1997;100:169-179.
20. Schoggins JW, MacDuff DA, Imanaka N, et al. Pan-viral specificity of IFN-induced genes reveals new roles for cGAS in innate immunity. *Nature*. 2014;505:691-695.
21. Rouhi L, Fan S, Cheedipudi SM, et al. Effects of tamoxifen inducible MerCreMer on gene expression in adult cardiac myocytes in mice. *The Journal of Cardiovascular Aging*. 2022;2.
22. Rouhi L, Cheedipudi SM, Chen SN, et al. Haploinsufficiency of Tmem43 in cardiac myocytes activates the DNA damage response pathway leading to a late-onset senescence-associated pro-fibrotic cardiomyopathy. *Cardiovasc Res*. 2021;117:2377-2394.
23. Auguste G, Gurha P, Lombardi R, Coarfa C, Willerson JT, Marian AJ. Suppression of activated FOXO transcription factors in the heart prolongs survival in a mouse model of laminopathies. *Circ Res*. 2018;122:678-692.
24. Devereux RB, Alonso DR, Lutas EM, et al. Echocardiographic assessment of left ventricular hypertrophy: comparison to necropsy findings. *Am J Cardiol*. 1986;57:450-458.
25. Yuan P, Cheedipudi SM, Rouhi L, et al. Single-cell RNA sequencing uncovers paracrine functions of the epicardial-derived cells in arrhythmogenic cardiomyopathy. *Circulation*. 2021;143:2169-2187.
26. Bergmann O, Zdunek S, Alkass K, Druid H, Bernard S, Frisen J. Identification of cardiomyocyte nuclei and assessment of ploidy for the analysis of cell turnover. *Exp Cell Res*. 2011;317:188-194.
27. Higo T, Naito AT, Sumida T, et al. DNA single-strand break-induced DNA damage response causes heart failure. *Nat Commun*. 2017;8:15104.
28. Rech L, Abdellatif M, Pottler M, et al. Small molecule STING inhibition improves myocardial infarction remodeling. *Life Sci*. 2022;291:120263.
29. Decout A, Katz JD, Venkatraman S, Ablasser A. The cGAS-STING pathway as a therapeutic target in inflammatory diseases. *Nat Rev Immunol*. 2021;21:548-569.
30. Cao DJ, Schiattarella GG, Villalobos E, et al. Cytosolic DNA sensing promotes macrophage transformation and governs myocardial ischemic injury. *Circulation*. 2018;137:2613-2634.
31. Hu D, Cui YX, Wu MY, et al. Cytosolic DNA sensor cGAS plays an essential pathogenetic role in pressure overload-induced heart failure. *Am J Physiol Heart Circ Physiol*. 2020;318:H1525-1537.
32. King KR, Aguirre AD, Ye YX, et al. IRF3 and type I interferons fuel a fatal response to myocardial infarction. *Nat Med*. 2017;23:1481-1487.
33. Burla R, la Torre M, Merigliano C, Verni F, Saggio I. Genomic instability and DNA replication defects in progeroid syndromes. *Nucleus*. 2018;9:368-379.
34. Graziano S, Kreienkamp R, Coll-Bonfill N, Gonzalo S. Causes and consequences of genomic instability in laminopathies: Replication stress and interferon response. *Nucleus*. 2018;9:258-275.
35. Graziano S, Coll-Bonfill N, Teodoro-Castro B, et al. Lamin A/C recruits ssDNA protective proteins RPA and RAD51 to stalled replication forks to maintain fork stability. *J Biol Chem*. 2021;297:101301.
36. Singh M, Hunt CR, Pandita RK, et al. Lamin A/C depletion enhances DNA damage-induced stalled replication fork arrest. *Mol Cell Biol*. 2013;33:1210-1222.
37. Yusufzai TM, Tagami H, Nakatani Y, Felsenfeld G. CTCF tethers an insulator to subnuclear sites, suggesting shared insulator mechanisms across species. *Mol Cell*. 2004;13:291-298.
38. Gomez-Herreros F, Zagnoli-Vieira G, Ntai I, et al. TDP2 suppresses chromosomal translocations induced by DNA topoisomerase II during gene transcription. *Nat Commun*. 2017;8:233.
39. Gao R, Schellenberg MJ, Huang SY, et al. Proteolytic degradation of topoisomerase II (Top2) enables the processing of Top2-DNA and Top2-RNA covalent complexes by tyrosyl-DNA-phosphodiesterase 2 (TDP2). *J Biol Chem*. 2014;289:17960-17969.
40. Austin CA, Lee KC, Swan RL, et al. TOP2B: the first thirty years. *Int J Mol Sci*. 2018;19(9):2765.
41. Gibbs-Seymour I, Markiewicz E, Bekker-Jensen S, Mailand N, Hutchison CJ. Lamin A/C-dependent interaction with 53BP1 promotes cellular responses to DNA damage. *Aging Cell*. 2015;14:162-169.

KEY WORDS cardiomyopathy, DNA damage, genome instability, heart failure, lamin A/C

APPENDIX For supplemental tables, please see the online version of this paper.